DE-EE0006816.0000
Oregon State University
Advanced Laboratory and Field Arrays (ALFA) for Marine Energy

1. INTRODUCTION

The function of anchoring systems in marine energy applications is to withstand the extreme environmental loadings and keep wave energy converters (WEC) in position. A variety of anchoring devices are used in practice to secure the mooring lines to the seabed. According to their positions and behaviors, the anchoring systems can generally be divided into two categories: gravity anchors and embedded anchors (Randolph and Gourvenec 2011). Gravity anchors generate holding capacity by the self-weight of the anchors and the friction between anchor and seabed. However, due to their limited practical size and thus, holding capacity, gravity anchors can only be used in relatively shallow water. Embedded anchors can provided more holding capacities compared to gravity anchors which are, therefore, commonly used in both shallow and deep waters.

There are several different types of embedded anchors, including anchor piles, suction caisson anchors, drag anchors, suction embedded plate anchors (SEPLA) and dynamically penetrated anchors (DPA). These anchors have been previously studied with results reported in the offshore and geotechnical engineering literature (e.g. Lieng et al. 1999, 2000; Medeiros 2002; O'Loughlin et al. 2004; Richardson et al. 2009). Anchor pile behavior is similar to the pile behavior for on-shore deep foundations. Suction caisson anchors have similar bearing behavior to piles, with the bearing/holding capacity mainly contributed by the interface friction between the pile shaft and the surrounding soils (Salgado 2008). SEPLAs are a specific form of plate anchor which are embedded into the seabed by suction caisson (El-Sherbiny 2005; Gaudin et al. 2006; Yang et al. 2011). The plate anchor is then keyed by the anchor chain resulting in the plate rotating to be normal to the mooring line (Valent et al. 1979). After being keyed, SEPLAs perform similarly to ground plate anchors. DPAs are anchors that embed themselves into the seabed under free-fall (Lieng et al. 1999, 2000; Medeiros 2002). Physical experiments and analytical analyses have been used to study the behavior of plate anchors and DPAs for decades (e.g. Meyerhof and Adams 1968; Vesic 1969; Das and Seeley 1975; Rowe and Davis 1982; Chattopadhyay and Pise 1986; Murray and Geddes 1987; Dickin 1988; Rao and Kumar 1994; Merifield and Sloan 2006; Kumar et al. 2008; O'Loughlin et al. 2009; Koprivica 2009; Liu et al. 2011; Liu et al. 2013; Hanna et al. 2015). These studies have considered anchor behaviors as a function of a variety of variables, e.g. embedment ratio, soil density, anchor roughness, and soil type, and have been seen to respond in manners similar to those observed in bulk soils and other geostructures. Plate anchors embedded in dense soils, for example, exhibit material hardening behavior followed by softening during uplift, consistent with observations from element-scale laboratory tests on soils, such as triaxial tests and direct shear tests.

This report presents results from discrete element method (DEM) simulations of the behavior of embedded plate anchors during uplift in granular soils. DEM allows for the simulation of soils as a collection of individual particles (Cundall and Stack 1979) and has been applied to a wide range of problems involving granular materials interacting with structures (e.g., Frost et al. 2002; Kress and Evans

2010; Evans and Kress 2011). DEM models predict the emergent behavior of particulate assemblies (e.g., sands) based on simulation of independent particle behaviors. In marine systems, the interaction between seabed sands and offshore anchors is one specific example of soil-structure interaction. The properties of the seabed and the anchor combine to determine the holding capacity and allowable reaction force for a given anchor design. Most of the previous research on plate anchors has been based on physical experiments and analytical analyses (e.g. Meyerhof and Adames 1968; Murray and Geddes 1987; Dickin 1988). However, many of the microscale behaviors occurring at the anchor-soil interface are barely considered to assess the potential of material softening behavior in MHK systems. The current work employs DEM simulations using the software *PFC*^{3D} (Itasca 2008) to evaluate the effects of soil properties and anchor surface roughness on holding capacity and to investigate the micromechanics of anchor uplifting. By better understanding the fundamental particle-scale soil response during uplift, it may be possible to better extrapolate results from physical experiments to a wider variety of anchor-seabed combinations.

2. SIMULATION OF SUCTION EMBEDDED PLATE ANCHOR

2.1. Model Overview

The geometry of the DEM model of the embedded plate anchor is shown in Figure 1. The plate anchor is modeled as a rigid monolayer of small particles arranged on a simple cubic lattice. As shown in the figure, the diameter of plate anchor particle is $0.05D_{50}$, where D_{50} is the mean particle size of the surrounding assembly. Particle properties are exactly the same as those used for all previous simulations in this project (e.g., the Year 1 Annual Report). The plate anchor has a dimension of $0.2W \times 0.2L \times d$, where W and L are the width and length of the granular assembly, respectively, and d is the diameter of the particles used to construct the plate anchor. The height of the granular assembly is H.

An assembly of polydisperse spherical particles is generated to fill the model volume in the box at a user-defined porosity. Mass scaling (e.g., Belheine et al. 2009; Evans and Valdes 2011) was employed to decrease simulation time; as such, the mean model particle diameter is $D_{50} = 0.4m$ and other model dimensions are scaled accordingly. Specifically, model height (H), model width (W), and model length (L) can be expressed in terms of D_{50} as $H = 50D_{50}$, $W = 37.5D_{50}$, and $L = 37.5D_{50}$, respectively.

Previous research on the shear strength of granular soils has shown that shear band thickness is approximately 8-10 times median particle diameter (e.g., Mühlhaus and Vardoulakis 1987; Frost et al. 2004). Thus, the distance between the edges of plate anchor and outside walls was set to be as $0.4 \times W/D_{50} = 15D_{50}$. Moreover, according to Dickin (1988), the soil beneath the anchor has little influence on the anchor capacity, so the distance between plate anchor and bottom wall may thus be set to a relatively small value. Previous experimental studies have focused on anchor holding capacity as a function of anchor embedment depth (Rowe and Davis 1982; Murray and Geddes 1987; Dickin 1988; Merifield and Sloan 2006) and the relationship between embedment ratio and breakout factor. Embedment depths can be modeled by changing the plate position in the simulations.

The DEM model consists of spherical particles and boundary walls. The model variables and material properties are shown in Table 1. Material properties were selected to be consistent with physical properties of silica sands previously published in the literature. However, it is possible to vary these parameters in order to simulate other soil types (e.g., carbonate sands) or to calibrate the model to observed response while still remaining within the range of physically-realistic material properties.

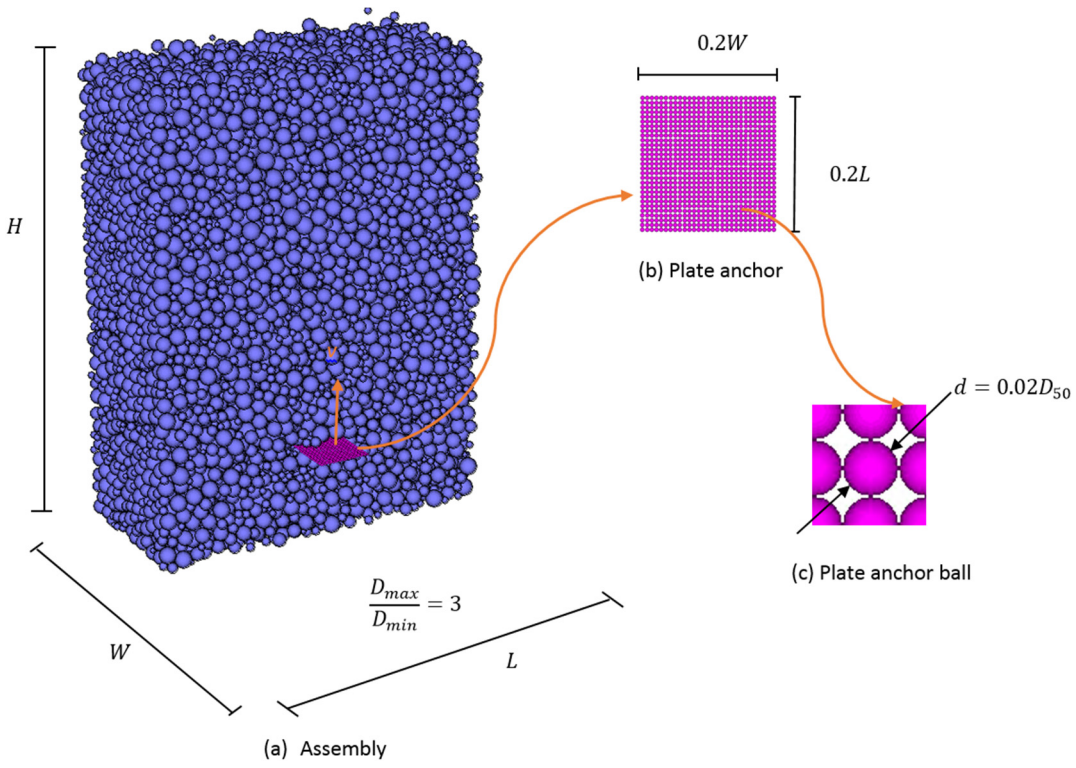

Figure 1. Geometry of the DEM model (particle assembly shown in section with half of particles removed to reveal embedded plate anchor)

The standard spring/linear contact model was used in all the simulations. Contacts between particles and particles or between particles and walls are considered as springs in both normal and shear directions. Particles were assigned normal and shear stiffnesses based on the Potyondy stiffness in the Hertz-Mindlin contact for quartz material (Potyondy and Emam 2004). Contact forces and unbalanced forces of all the particles can be obtained according to force-displacement law and Newton's second law. Physical constants used in the simulations include- soil density, normal stiffness, shear stiffness and inter-particle friction coefficient. The material and model properties are listed in Table 1.

A numerical servo-control mechanism is used to consolidate the specimen such that it is in numerical equilibrium at a specified isotropic stress state with a tolerance of 0.5% by adjusting the positions of the plate walls. The porosity of the consolidated assembly can be adjusted by varying the particle and wall friction coefficients during assembly generation and consolidation, with a lower friction coefficient resulting in a denser specimen. After consolidation, particle friction can be adjusted to assess the effects of particle friction of anchor pullout resistance. The top wall is removed to model uplift in soils with a free surface. The specimen is then re-equilibrated, and finally, a constant upward velocity is applied to the anchor plate while the remaining specimen boundaries are held fixed. To monitor particle responses during anchor uplift, 100 measurement spheres are randomly generated in the specimen with a diameter of twice the maximum particle size $2D_{max}$. (Note that these measurement spheres are simply convenient

regions over which model response may be averaged.) The anchor holding capacity is the out-of-balance force on the plate anchor.

Table 1. Material and model properties.

	Parameter	Value
Particles	Particle diameter ratio[(1)], d_{max}/d_{min} [ ]	3
	Normal stiffness, k_n [N/m]	1×10^8
	Shear stiffness, k_s [N/m]	8×10^7
	Friction coefficient, μ [ ]	0.50
	Density, ρ_s [kg/m^3]	2650
Model	Height, H [d_{50}]	50
	Width, W [d_{50}]	37.5
	Length, L [d_{50}]	37.5
	Wall stiffness, k_w [N/m]	2×10^8
	Initial porosity [ ]	0.40
Plate Anchor	Normal stiffness, k_{pn} [N/m]	1×10^8
	Shear stiffness, k_{ps} [N/m]	8×10^7
	Particle diameter, d [d_{50}]	0.02
	Width, w [d_{50}]	6
	Length, l [d_{50}]	6

[(1)]Particle diameters are uniformly distributed between $\boldsymbol{d_{min}}$ and $\boldsymbol{d_{max}}$.

2.2. Parametric Analyses

A total of 16 simulations are performed to investigate the uplift behavior of a plate anchor considering factors including embedment depth, soil density, and anchor roughnesses. Five triaxial shear simulations were also performed to measure the bulk shear strength of the simulated material. Details of the simulation are listed in Table 2. The embedment ratio is defined as the embedment depth over anchor width ($\lambda = z_e/B$), z_e is the embedment depth and B is the anchor width. The embedment ratio ranges from 4.0 to 6.67. Anchor roughness was modeled by setting different particle friction coefficients of anchor particles for very smooth ($\mu_a = 0.0$) to very rough particles ($\mu_a = 0.5$). Soil porosity in the simulations range from 0.387 for relatively dense assemblies to 0.432 for very loose assemblies. The corresponding internal friction angles are measured by triaxial numerical simulations.

Breakout factors for the plate anchor are quantified in the simulations. The definition of breakout factor is the peak uplift resistance over the soil weight in free field, as shown in Equation 1.

$$c = \frac{P_{peak}}{\gamma z_e A} \tag{1}$$

where P_{peak} is the peak resistance, γ is the unit weight, z_e is the embedment depth and *A* is the anchor area. Besides the breakout factor, failure displacements for all simulations are quantified as well. In order to make them dimensionless, failure displacements are normalized by the plate width and defined here as relative failure displacement. Breakout factor together with relative failure displacement are determined herein as the pullout capacity factors for future comparison.

Table 2. Variables in the parametric analysis.

	Embedment ratio (λ)	Particle friction (μ_p)	Anchor particle friction(μ_a)	Void ratio
1	6.67	0.6	0.6	0.71
2	6.50	0.6	0.6	0.71
3	5.50	0.6	0.6	0.71
4	5.00	0.6	0.6	0.71
5	4.50	0.6	0.6	0.71
6	4.00	0.6	0.6	0.71
7	6.67	0.5	0.0	0.71
8	6.67	0.5	0.2	0.71
9	6.67	0.5	0.3	0.71
10	6.67	0.5	0.4	0.71
11	6.67	0.5	0.5	0.71
12	6.67	0.5	0.0	0.63
13	6.67	0.5	0.0	0.67
14	6.67	0.5	0.0	0.71
15	6.67	0.5	0.0	0.73
16	6.67	0.5	0.0	0.76

3. RESULTS AND DISCUSSION

Both large-scale response of granular material and microscale data are obtained via DEM simulations to investigate the influences of impact factors mentioned above on the bulk granular material. Knowledge of granular material response can be helpful for understanding uplift behavior in practice from a micromechanical point of view. The following paragraphs will focus on the simulation data from parametric analyses considering embedment ratio, anchor roughness, and soil density.

3.1. Effects of embedment ratio (λ)

The embedment ratio is defined previously as the ratio of embedment depth to anchor width. There are 6 different embedment ratios being simulated to investigate the influence of embedment ratio on the anchor pullout behavior (Table 2, simulations 1-6). The anchor resistance factor C_c was used to describe the magnitude of anchor resistance:

$$C_c = \frac{R}{\gamma z_e A} \tag{2}$$

where R is the anchor resistance, γ is the unit weight, z_e is the embedment depth and A is the area of the plate anchor.

For heterogeneous materials, failure will occur due to distributed damages during which the material has strain softening. Strain softening is a phenomena wherein stress will decline with increasing strains. The major causes of strain softening are heterogeneity and brittleness. Sand is a heterogeneous material. The stress in a sand assembly is transmitted by contacts among sand particles. The mechanism of strain softening consists of void redistribution or a loss of interparticle contacts. Strain softening stably exists in a certain region in the material within a well-defined shearing zone.

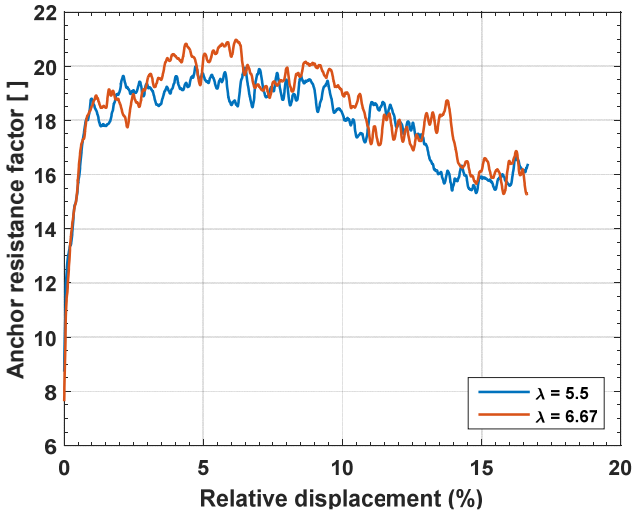

Figure 2. Anchor resistance factor as a function of relative failure displacement

Material softening in granular assemblies can be seen when the embedment ratio is equal to 5.5 and 6.67, for instance, in Figure 2. The relative displacement was defined as the ratio of anchor vertical displacement to anchor plate width. The maximum anchor resistance factor is the breakout factor defined Equation 1. The corresponding relative displacement is the relative failure displacement. Figure 3 shows the anchor resistance as a function of embedment ratio. It is clear that the breakout factor increases with increasing embedment ratio. Figure 4 shows the relative failure displacement as a function of embedment ratio. Relative failure displacement is found to be larger for larger embedment ratios as well.

The breakout factor c, which is also defined by other researchers as the dimensionless load coefficient (Murray and Geddes 1987), is one factor to describe anchor resistance. Due to strain softening, load will decrease after some maximum and thus, the peak resistance corresponds to the maximum holding capacity. It is clear that a larger embedment ratio implies a greater soil weight in the free field and a larger holding capacity when multiplied the relative larger breakout factor. For relatively deep anchors with λ from 4 to 6.67, the breakout factors range from 16 to 23, which is consistent with results from physical experiments (e.g., Meyerhof and Adams 1968; Rowe and Davis 1982; Dickin 1988), as discussed subsequently in Section 4. Relative failure displacements range from 0.23% to 2.63%.

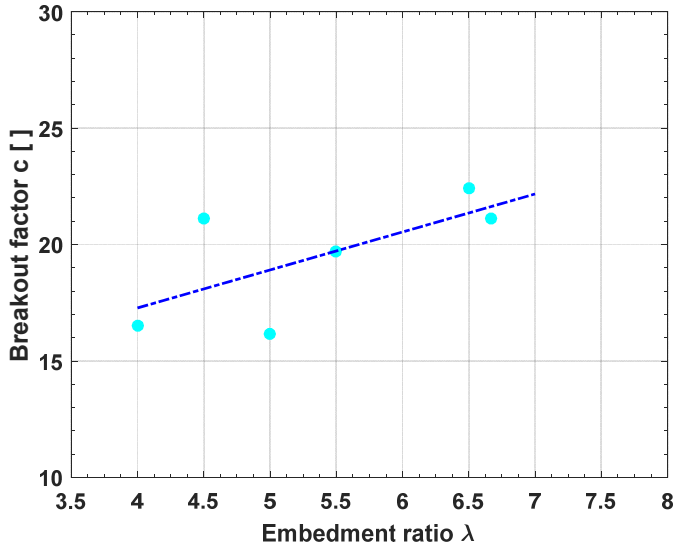

Figure 3. Breakout factor as a function of embedment ratio

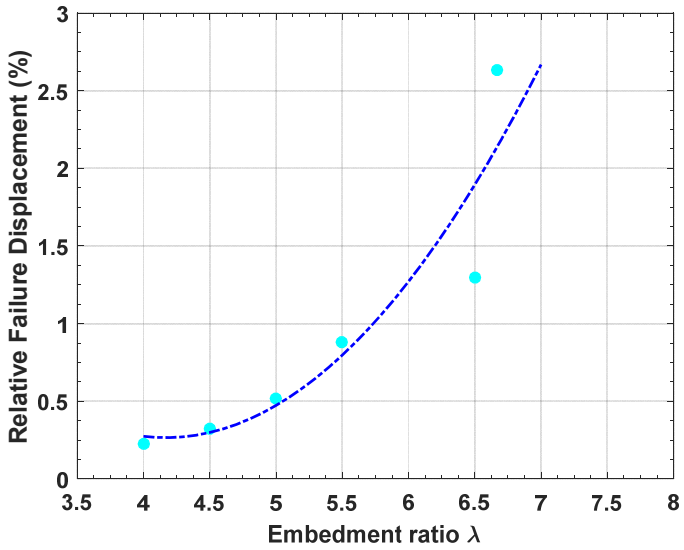

Figure 4. Relative failure displacement as a function of embedment ratio

3.2. Effects of anchor roughness (μ)

Friction is the shear resistance that occurs at a spatial scale much smaller than the median particle diameter and roughness is the shear resistance that manifests at the scale of the median particle diameter. Under this meaning, changing the friction of the anchor particles corresponds to changing the anchor roughness at very small scales.

To assess the effects of changing plate anchor friction, simulations were performed using an embedment ratio of 6.67 and with varying anchor particle friction from 0.0 to 0.5. Figure 5 shows anchor resistance versus relative anchor displacement for different anchor frictions. The results show that anchor roughness

has little effect on the resistance of plate anchors: the trends are similar, the breakout factors are similar (Figure 6), and the relative failure displacements are close to each other (Figure 7). The breakout factors for different anchor friction coefficients have a narrow range from 15.9 for the smooth anchor to 16.5 for the relatively rough anchor. Plate anchors do not rely upon frictional shear to provide pullout resistance. Anchor plate resistance for different anchor roughnesses from the DEM simulations are similar to observations from previous researchers based on physical experiments (e.g., Rowe and Davis 1982; Murray and Geddes 1987; Dickin 1988; Merifield and Sloan 2006).

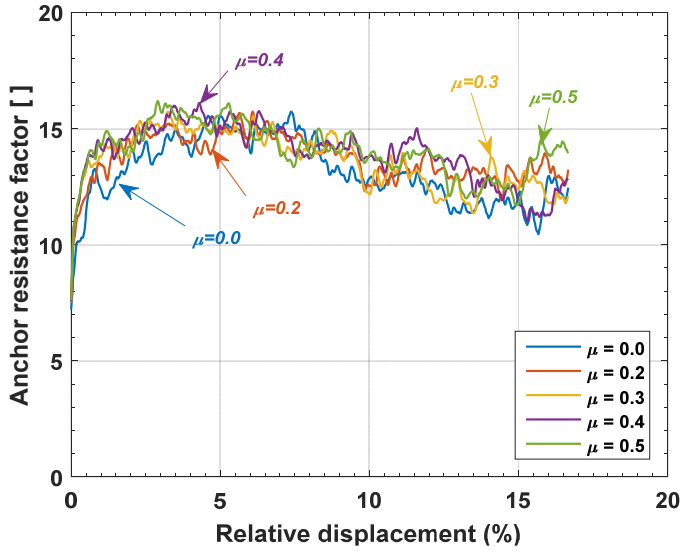

Figure 5. Anchor resistance as a function of relative displacement under different anchor frictions

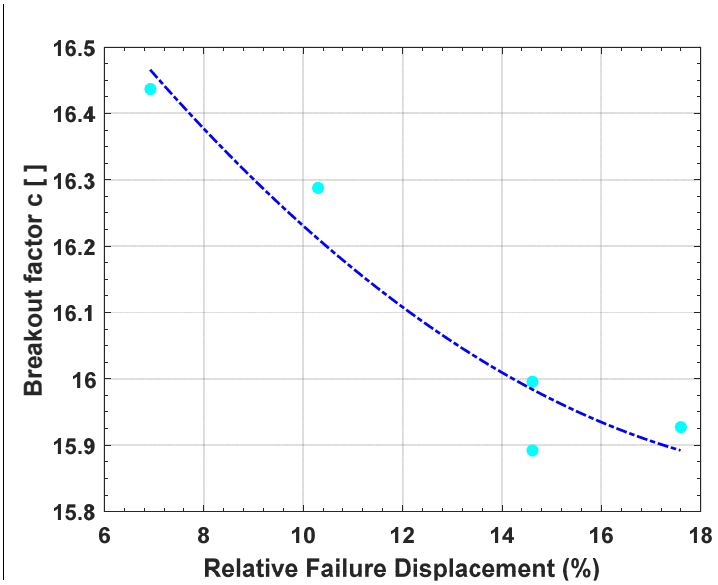

Figure 6. Breakout factor as a function relative failure displacement under different anchor frictions

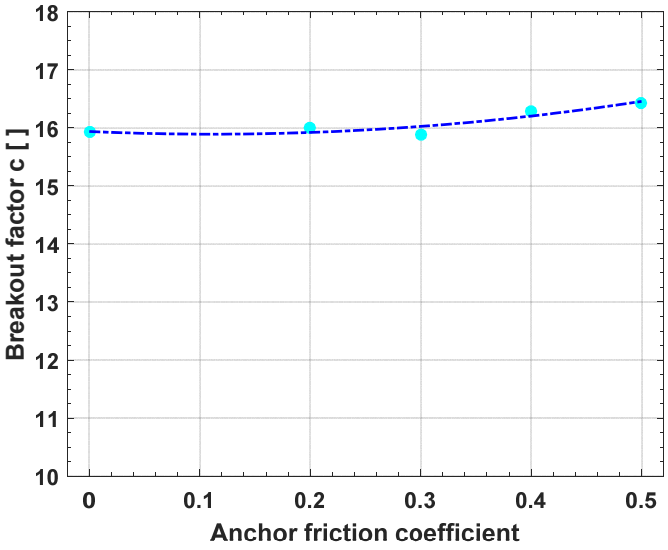

Figure 7. Breakout factor under different anchor friction coefficients

3.3. Effects of soil density

As mentioned previously, soil density can be adjusted by varying the particle and wall friction coefficients during assembly generation and consolidation, with a lower friction coefficient resulting in a denser specimen. To study the effects of soil density on pullout resistance, a set of simulations with void ratio ranging from e = 0.63 to e = 0.76 were performed. The void ratio is defined as the ratio of void volume to the solid volume of the assembly. The anchor resistance factor as a function of relative displacement for different porosities are shown in Figure 8.

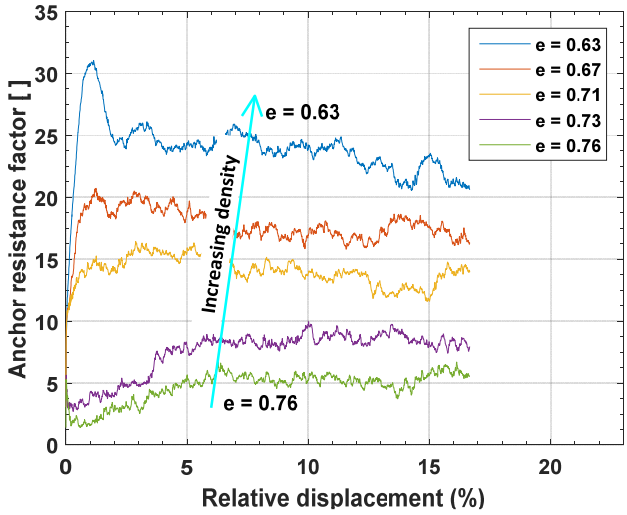

Figure 8. Anchor resistance factor along with relative displacement under different soil densities

Figure 8 shows that very dense assembly during anchor uplifting has an obvious material softening behavior following a sharp material hardening behavior. For looser assemblies, the peak anchor resistance factor is less obvious. There are no material softening behavior for the loosest assemblies; instead, the anchor resistance factor increases gradually to a relatively constant value.

To investigate the influence of soil density on the anchor pullout behavior, we use the measure relative density to help quantify the soil state:

$$D_r = \frac{e_{\max} - e}{e_{\max} - e_{\min}} \tag{3}$$

where e_{min} and e_{max} are the minimum and maximum void ratios, respectively. The meaning of maximum void ratio e_{max} and minimum void ratio e_{min} in the simulations are different from the values from experiments. In the models, e_{min} and e_{max} are used here as the minimum and maximum void ratios obtained from the simulations, respectively. Relative density is normalized in the range of $[0,1]$, (i.e. minimum porosity corresponds to $D_r = 1.0$ and maximum porosity corresponds to $D_r = 0.0$). Figure 9 shows clearly that breakout factor increases with relative density. The relationship is linear from a value of $c = 6$ for the loosest assembly to $c = 31$ for the densest. Soil density significantly influences the anchor behavior and the anchor holding capacity.

However, the relative failure displacement has an inverse correlation with relative density compared to breakout factor. In other words, a loose assembly has a larger relative failure displacement and a dense assembly has a smaller relative displacement. The relationship between relative failure displacement and relative density is shown in Figure 10. Murray and Geddes (1987), Dickin (1988) both report similar observations for physical systems. To better understand this behavior, it is necessary to consider pullout parameters as functions of soil shear strength rather than relative density, as discussed subsequently.

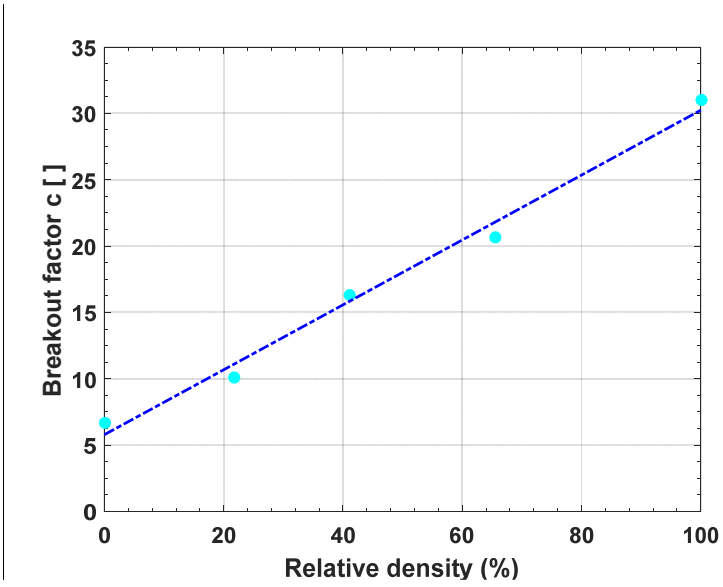

Figure 9. Breakout factor as a function of relative density

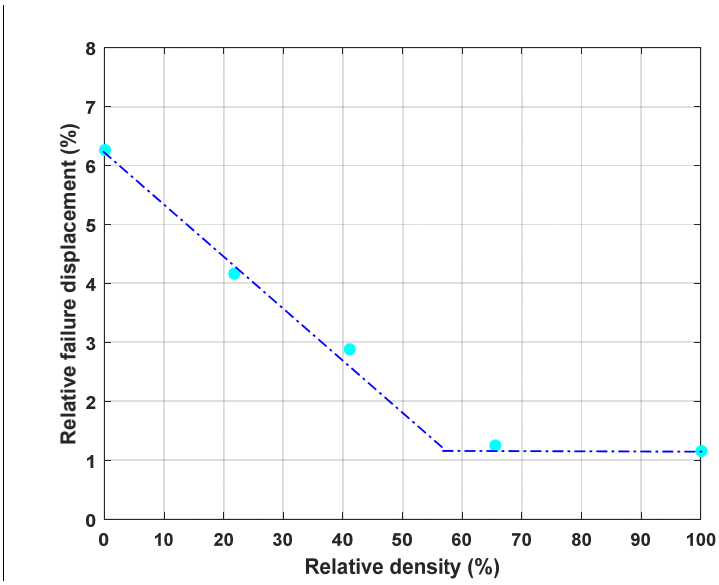

Figure 10. Relative failure displacement as a function of relative density

Five triaxial compression tests were performed on granular assemblies with exactly the same particle properties to measure shear strength. Soil shear strength can be affected by many factors, including soil type, soil density, and confining stress. The only factor varying across the five tests is specimen porosity (density). Under the same lateral confining stress, dense assemblies tend to dilate while loose assemblies tend to contract during shearing. The measured shear strengths, quantified as the angles of internal friction (e.g., Lambe and Whitman, 1968), are used as the strength descriptor for the following analyses of plate anchor pullout.

The shear strength of the soil, in the form of the internal friction angle, was normalized in a manner similar to that used for relative density:

$$\phi_r = \frac{\phi - \phi_{\min}}{\phi_{\max} - \phi_{\min}} \tag{4}$$

where ϕ_{min} and ϕ_{max} are minimum and maximum internal friction angle, respectively. Figure 11 clearly shows that under the same embedment ratio, a higher internal friction angle results in higher anchor resistance. According to the Mohr-Coulomb failure criterion, soils with higher shear strength have a higher internal friction angle. Therefore, soil strength is significantly influence the anchor uplifting resistance.

The relationship of relative failure displacement for different normalized friction angles is shown in Figure 12. The relative failure displacement for small internal friction angle is the largest. Relative failure displacement decreases with increasing internal friction angle. The bilinear behavior may be more readily interpreted when the independent variable is shear strength rather than density (i.e., Figure 10). Figure 12 implies significant deformation is required to mobilize shear strength in the absence of dilation (which is a contributor to shear strength). However, when a significant portion of anchor resistance is due to volumetric dilation, relatively less deformation is needed to fully mobilize shear strength. This is consistent with the existing state of knowledge on the shear strength of granular materials and, perhaps more

significantly, also with the granular-continuum interface shear simulations reported previously (Evans and Zhang 2015; Zhang and Evans 2016). The break point in the bilinear trend in Figure 12 corresponds to the transition from contractive to dilatant behavior – this is, it can be considered a point on the critical state surface for this particular material and anchor model.

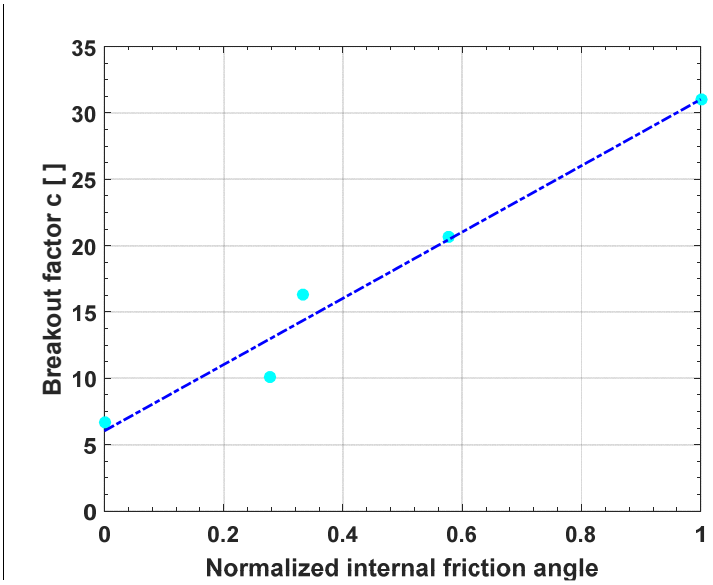

Figure 11. Breakout factor as a function of normalized internal friction angle

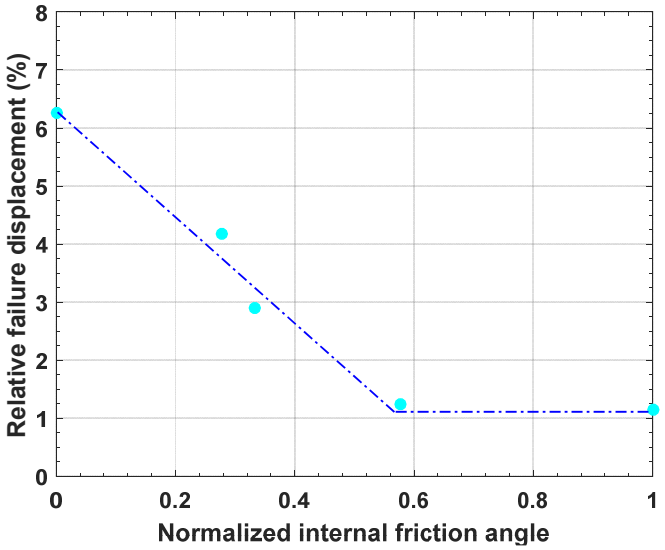

Figure 12. Relative failure displacement as a function of normalized internal friction angle

4. COMPARISON WITH PUBLISHED EXPERIMENTAL TESTS

Comparisons to physical experiments reported in the literature are used to evaluate the validity of the DEM model. Square anchor plate pullout tests performed by Meyerhof and Adams (1968), Rowe and Davis (1982), Dickin (1988) and Rao and Kumar (1994) were used for comparison. For similar material densities for sands and idealized granular materials, breakout factors ranging from 10 to 30 were found from physical experiments. The DEM simulations also gave a similar range to the experimental test shown in Figure 13.

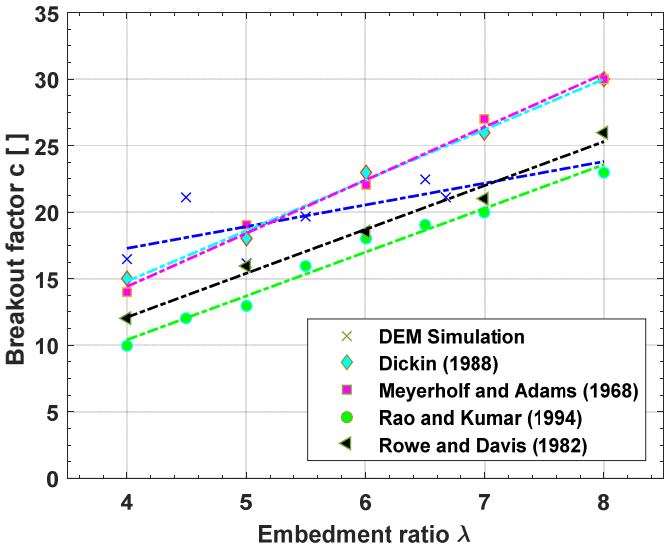

Figure 13. Comparisons of breakout factors along with embedment ratio between experimental tests and DEM simulation

The failure displacement data extracted from the literature are used for comparison to the DEM simulations. Instead of comparing the relative failure displacement directly, the relative failure displacements under different embedment ratios are normalized as:

$$\delta = \frac{\delta_{relative}}{\delta_{\lambda=6.67}} \tag{5}$$

where $\delta_{relative}$ is the relative failure displacement, $\delta_{\lambda=6.67}$ is the relative failure displacement at an embedment ratio of 6.67. Figure 14 shows that normalized relative failure displacements for DEM simulations are smaller than the experimental results for relatively shallow embedment depths; however, simulated normalized relative failure displacement for deeper embedments are consistent with those from physical experiments. This behavior is likely due to the idealized spherical particle shapes used in the DEM simulations. There spheres have no interlocking between particles other than that due to surface friction. Significant particle rotation during uplift will result in lower normalized relative failure displacement, with this effect being more prominent at lower confining stresses (i.e., embedment ratios).

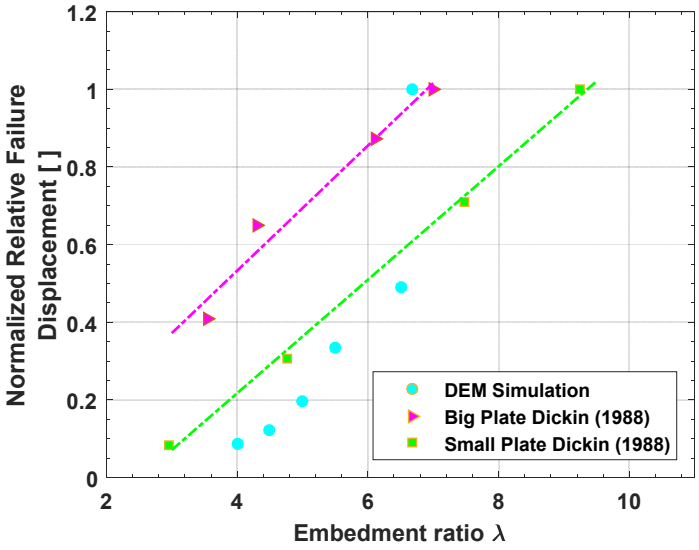

Figure 14. Comparisons of normalized relative failure displacement along with embedment ratio between experiment tests and DEM simulation

5. MICROSCALE INVESTIGATION

In addition to the macroscale response, in which the granular material was considered to behave as a continuum and relative movements and rotations of particles were not considered (O'Sullivan 2011), a microscale analysis of the granular assembly was performed. Directional fabric parameters (e.g. contact orientation), anisotropy, and coordination number were measured and quantified and are discussed in the following subsections.

5.1. Contact orientation

Four different stages of pullout were considered in the analysis of contact orientations: (1) prior to uplift; (2) at the onset of compression; (3) anchor breakout; and (4) at critical state. For a three-dimensional assembly, contact orientation has three components: the x, y and z directions. The inclination angle (ψ), also called the zenith angle, is defined as the angle between orientations projected to x-z or y-z plane and x-y plane. Figure 15 presents the contact normal inclination (zenith angle) distribution for both dense (e = 0.63) and loose (e = 0.73) assemblies.

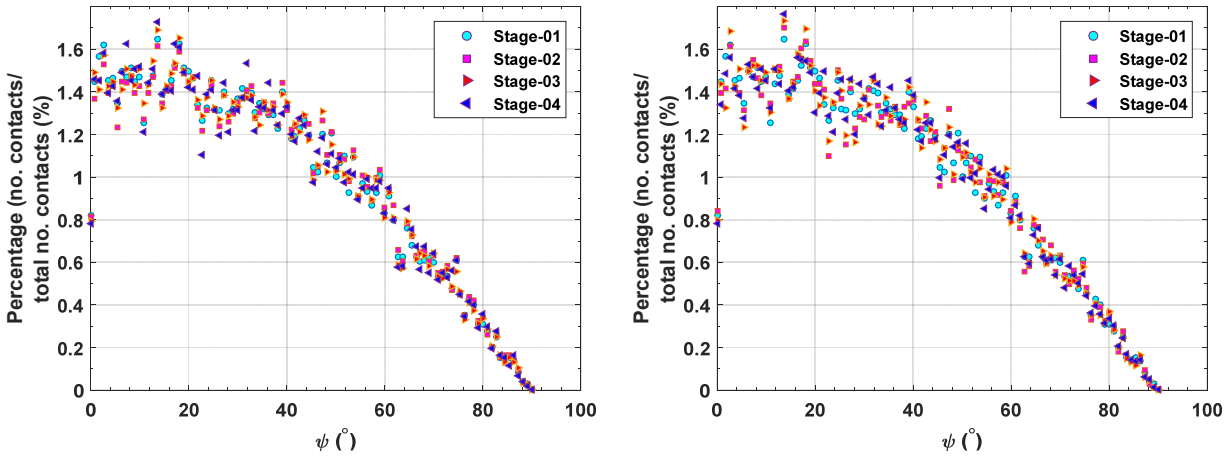

Figure 15. Contact normal orientation (ψ inclination) distribution for dense (L) and loose (R) assemblies

For the dense assembly at Stages (1) and (2), very few contacts have an inclination of ψ>60°. However, the number of contacts with inclinations of ψ>60° increases substantially in Stages (3) and (4). There is a clear reorientation of the contact normal orientations towards the vertical. Vertical translation of the plate anchor re-orients the surrounding contacts among particles. The behavior is similar for both dense and loose assemblies, but the phenomenon is less obvious for the loose assembly.

In addition to the contact orientation distribution shown in Figure 15, the normal forces carried by those contacts are part of the fundamental particle-scale mechanics that are governing overall material behavior. Contact normal force distributions are presented in log-linear and log-log scales for the four stages defined above are presented in Figure 16. The forces are normalized by the mean normal force ($\bar{f}_n$) for each stage. Azema et al. (2007) found that the number of strong forces (above $\bar{f}_n$) falls off exponentially as follows:

$$P(f_n) \propto e^{-\alpha_1 f_n/\bar{f}_n} \tag{6}$$

where α_1 is a coefficient defining the width of the distribution and is related to particle shape, among other parameters. Based on the theory developed by Azema et al. (2007), the α_1 coefficients for the assemblies are 1.05 and 0.97 at anchor breakout for the dense and loose assemblies, respectively. A smaller value corresponds to a wider distribution, which is evident from Figures 16(a) and (b) which show visibly that the dense assembly is narrower than the loose assembly. The distribution of normalized contact forces has a similar pattern for both dense and loose assemblies. However, for the dense assembly, Stage (4) has a noticeably larger fraction of high contact forces than the other stages.

Contact forces at critical state distribute in a higher value range which is different from the state prior to uplifting, or onset of uplifting, of which the values distribute in a lower value range. Loose assembly gives a similar but obvious phenomenon, i.e. contact forces prior to pullout have a smaller frequency comparing to other following stages. This phenomenon is more readily observed through log-log scale plots, Figures 16(c) and (d). Anchor movement results in contact force redistribution. This might be explained, loose assembly for example, the out-of-balance force of plate anchor (clump) is very small under a lower

average ratio 10^{-4}. Therefore contact normal forces are very small to meet the equilibrium, contact forces distribute in the smaller value range, see Figure 16 (b) and (d).

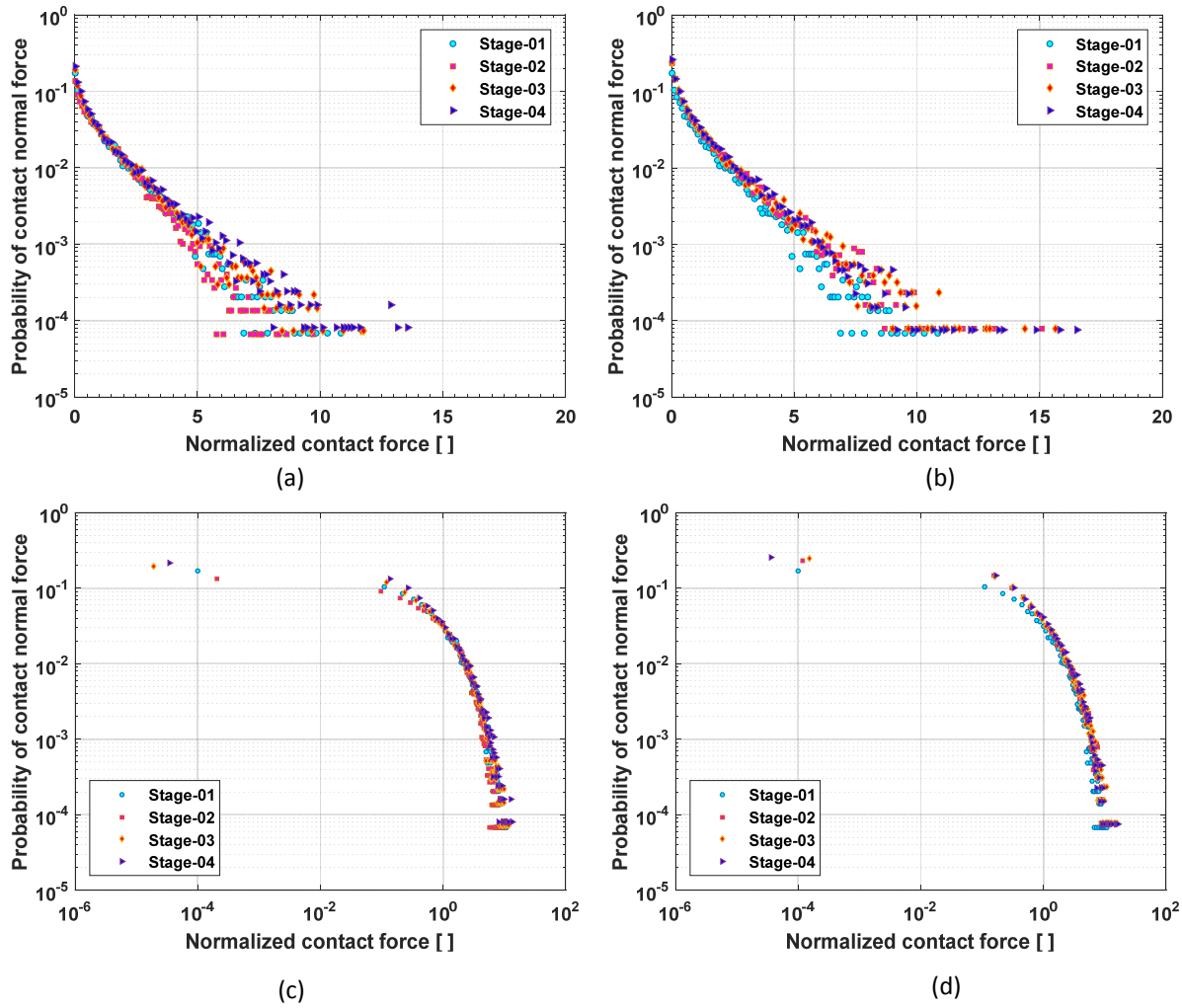

Figure 16. Contact normal force distributions of dense and loose assemblies, a, c are dense assembly, b, d are loose assembly.

The contact force chains, which may be visualized as lines connecting the centroids of all contacting particles in the assembly, are shown in Figure 17 for the breakout load with an embedment ratio of $\lambda = 6.67$. The thickness of an individual contact force chain is proportional to the magnitude of the contact force, which shows that the particles above the plate anchor contribute to the anchor holding resistance. Under both gravity and the forces applied by the plate anchor, the contact forces among particles above the plate are redistributing, increasing, and transmitting to the particles nearby to form a "contact force chain tree" until the breakout point (shown in Figure 17). The colored particle velocities on the right in Figure 17 show that, via Newton's second law and the force-displacement law, the particle velocities are transmitting from the plate anchor to the particles within (and beyond, in some cases) the failure zone. In previous work, an embedment depth of $\lambda = 6.67$ is typically assumed to be a "deep" plate anchor, though

this designation has not been otherwise quantified. However, from an analysis of contact-level forces in the model, it is clear that the contact force chain tree does not reach the free surface at the point when the granular assembly fails (i.e., at the breakout force). This significant finding implies that there is a reasonable metric by which to delineate “shallow” versus “deep” anchor behaviors for use in design.

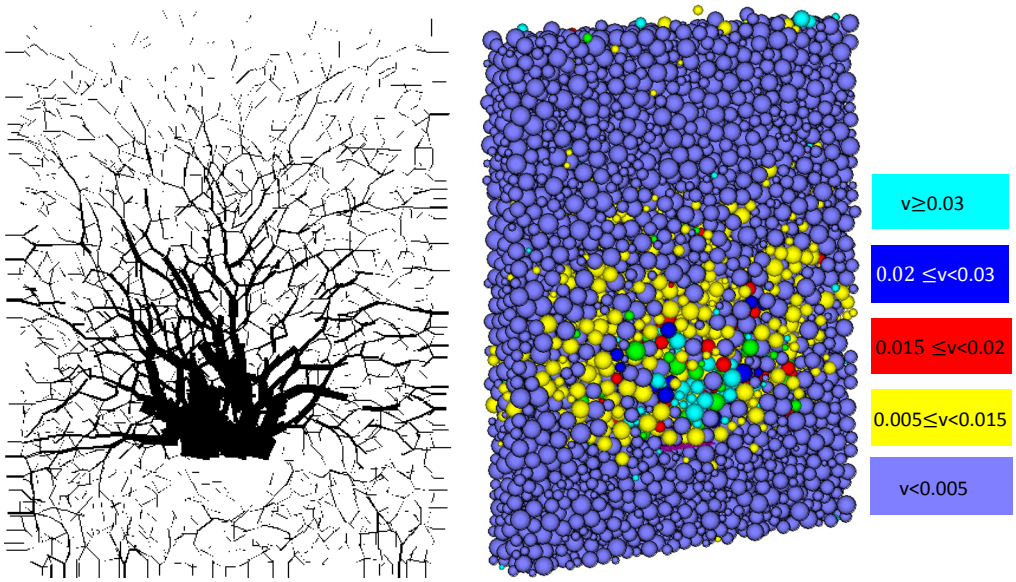

Figure 17. Contact force chain (left) and colored particle velocity vector (right) of dense assembly at peak

5.2. Anisotropy

Anisotropy in granular assemblies is classified into three different types – inherent, induced, and initial anisotropy (Barreto, 2010). Inherent anisotropy develops during deposition and is influenced by the source material of the deposit and the geometry of the grains. Initial anisotropy develops both during deposition and over the geological stress history of the deposit (O’Sullivan 2011). The induced-anisotropy first defined by Casagrande and Carrillo (1944) is the strain- or stress-induced particle reorientations. Directional parameters can be used to describe the directional fabric, as first proposed by Oda (1977). Soil fabric is used to represent the arrangement of particles and associated voids in a soil mass (Yimsiri and Soga 2001). The fabric tensor is commonly used to describe the directional parameters and the preferred orientation of a dataset of vectors (e.g., Rothenberg and Bathurst 1989; Wang et al. 2007; Fonseca et al. 2013a, 2013b). The fabric tensor defined through directional parameters (contact normal orientation) is shown as Equation 7:

$$\Phi_{ij} = \frac{1}{N}\sum_{k=1}^{N} n_i^k n_j^k \tag{7}$$

where N is the total number of contacts in the system and n_i^k is the unit contact orientation along the i direction. In three dimensions, the fabric tensor is second-order with nine elements. Contact normal orientation anisotropy is obtained through an eigenvalue analysis of the fabric tensor. The magnitudes of anisotropy can be calculated as the eigenvalues of the fabric tensor, i.e. the major fabric is given as Φ_1,

the minor fabric is Φ_3, and the intermediate fabric tensor is Φ_2, with the relationship as $\Phi_1 > \Phi_2 > \Phi_3$. The deviator fabric can be calculated as:

$$\Phi_d = \frac{1}{\sqrt{2}}\sqrt{\left(\Phi_1 - \Phi_2\right)^2 + \left(\Phi_2 - \Phi_3\right)^2 + \left(\Phi_3 - \Phi_1\right)^2} \tag{8}$$

where Φ_d is deviator fabric which is also defined as anisotropy.

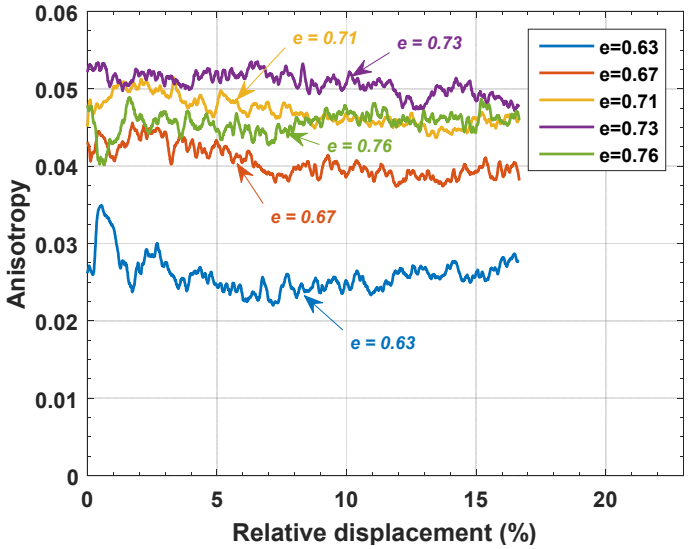

Figure 18. Contact normal anisotropy along with relative displacement for assembly with different void ratios

Figure 18 shows the contact normal anisotropy as a function of relative displacement. In the simulations, the initial value is explained by considering the gravity field and the assembly consolidation process. In another words, because of the existing gravity, the granular material is not isotropic. Gravity and subsequent isotropic consolidation are the major contributors to the initial and inherent anisotropies. After the plate anchor begins moving, the plate movements will re-orient the particles above the plate. In the dense assembly, there is a strain-hardening behavior in the anisotropy, similar to that observed in the anchor resistance (Figure 8). After failure (breakout), the particle contacts will re-orient under both gravity and the uplifting force. The magnitudes of anisotropy are at the same level as the initial value, which implies that after the granular assembly fails, the uplift forces will not be a major contributor to the induced anisotropy as during the onset of pullout. However, for the loose assembly, there is no corresponding hardening behavior in the anisotropy, similar to the anchor resistance behavior during pullout (Figure 8). The initial anisotropy is much larger than that in the dense assembly, implying that fabric is a contributor to pullout resistance, but not the sole governing factor.

5.3. Coordination number

The coordination number quantifies the number of contacts per particle in the material and is a measure of the packing density at the particle scale. The definition of coordination number is:

$$CN = \frac{2N_c}{N_p} \tag{9}$$

where N_c is the total number of contacts and N_p is the number of particles. The coordination number is the most fundamental particle-scale measurement of the material and it is easy to obtain by DEM simulation (O'Sullivan 2011). The evolution of coordination number with increasing relative displacement for different densities is shown in Figure 19.

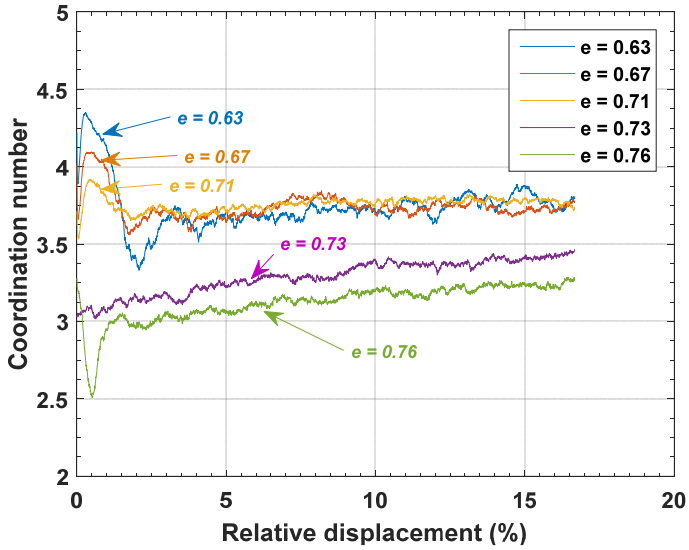

Figure 19. Coordination number along with relative displacement under different densities.

Figure 19 shows that for relatively dense assemblies, the coordination number increases at the start of pullout to a peak value followed by a decreasing behavior to a critical state, at which point the coordination numbers become nearly constant, independent of initial void ratio (for dense samples only). For looser assemblies, the coordination number generally increases slightly with relative displacement. In the loosest assembly, however, the coordination number drops sharply at the beginning of plate movement; this response can be attributed to local collapse of metastable fabric in the vicinity of the plate anchor.

6. SUMMARY AND CONCLUSIONS

Unlike previous work on soil behavior during anchor pullout, this study uses DEM modeling to show macroscale response of the anchor and the microscale mechanisms underlying the observed response. The macroscale analysis focuses on the influence of factors like embedment ratio, soil density, and anchor roughness on the anchor breakout factor during uplift. The particle-scale analysis focuses on the particle contact orientations, anisotropy, and coordination number and how those mechanisms can be used to explain the design-scale mechanics.

(a) For relatively deep anchors with embedment ratios from 4 to 6.67, the breakout factor ranges from 16 to 23 for the given conditions (anchor and soil properties). Simulated breakout factor magnitudes have as similar range to those obtained via physical experiments. Relative failure displacements have

a range from 0.23% to 2.63%. The granular assembly fails at low displacements for smaller embedment depths and at larger displacements for larger embedment depths.

(b) The breakout factors for different anchor friction coefficients (roughness at the microscale) range narrowly from 15.9 for a smooth anchor (friction coefficient of anchor balls equal to zero) to 16.5 for a relatively rough anchor (friction coefficient of anchor balls equal to 0.8). The influence of anchor roughness on the anchor resistance is small, but plate anchors do not rely upon interface friction to provide holding capacity.

(c) Higher relative densities result in larger breakout factors. The relationship increases approximately linearly from 6 for the loosest assembly (void ratio of 0.76) to 31 for the densest assembly (void ratio of 0.63). Soil density significantly influences the anchor behavior and anchor holding capacity.

(d) The relative failure displacement has an inverse correlation with density. That is, looser assemblies have a larger relative failure displacement than denser assemblies. This behavior coincides with the experimental results reported by previous researchers (e.g., Murray and Geddes 1987; Dickin 1988).

(e) Comparisons were made between DEM simulations and previous experimental tests focusing on two major measures of performance – breakout factors and relative failure displacement under different embedment ratios. In the DEM simulations, breakout factors for different embedment depths are found to be consistent with the physical experiments from the literature. However, due to the difference of plate anchor shapes between DEM simulations and experimental tests, the failure displacements from DEM simulations deviate with a small percentage, say 15% for relative failure displacement.

(f) For the contact normal orientations, there is a clear reorientation of the contact normals towards vertical during anchor pullout. Contact inclination ranges mostly from 0° to 60° prior to plate movement and ranges from 0° to 90° during pullout. This behavior is similar for both dense and loose assemblies.

(g) The distribution of normalized contact forces has a similar pattern for both dense and loose assemblies. However, for the dense assembly, Stage (4) exhibits larger probabilities for higher normalized contact forces. Contact forces at critical state distribute in a higher value range, which is different from the state prior to pullout where the values are distributed in a lower range.

(h) Anisotropies for the dense assemblies have a similar response pattern to the anchor resistance: a sharp hardening behavior towards breakout. The granular assembly after failure will reconsolidate and particle contacts will re-orientate under both gravity and the applied pullout force. The magnitudes of anisotropy are similar to the initial value. However, for loose assemblies, there is no obvious “hardening” of deviatoric anisotropy in the loose assemblies during pullout.

(i) For relatively dense assemblies, the coordination numbers increase at the start of plate motion, ultimately reaching a peak value, before decreasing to a critical state, at which point the coordination numbers are almost constant. For the looser assemblies, the coordination number increases gradually with relative displacement.

(j) From an analysis of contact-level forces in the model, the contact force chain tree does not reach the free surface at the point when the granular assembly fails (i.e., at the breakout force). This significant finding implies that there is a reasonable metric by which to delineate “shallow” versus “deep” anchor behaviors for use in design.

7. CONTINUING WORK

This report provides results from a large number of numerical simulations designed to study the behavior of plate anchors during pullout from granular soils. Model results are interpreted across multiple spatial scales. Moving forward, it is necessary to further synthesize our understanding of these results from the particle level to the design level. Specifically, the power of understanding system mechanics at the microscale is that it enables extrapolation of design-scale understanding to anchors, assemblies, and materials that have not been specifically considered in the current work. Developing a more robust interpretation of the microscale measurements is the subject of continuing work and will be described in detail in future reports.

8. REFERENCES

Andersen, K., A. Puech, and R. Jardine. Cyclic resistant geotechnical design and parameter selection for offshore engineering and other applications. *Design for cyclic loading: Piles and other foundations, Proceeding of TC 209 Workshop–18th ICSMGE*, Paris. 2013.

Azéma, E., Radjai, F., Peyroux, R., and Saussine, G. (2007). Force transmission in a packing of pentagonal particles. *Physical Review E*, 76(1), 011301.

Barreto, I. (2010). Dynamic capabilities: A review of past research and an agenda for the future. *Journal of Management*, 36(1), 256—280.

Belheine, N., Plassiard, J. P., Donzé, F. V., Darve, F., and Seridi, A. (2009). Numerical simulation of drained triaxial test using 3D discrete element modeling. *Computers and Geotechnics*, *36*(1), 320-331.

Casagrande, A., and Carillo, N. (1944). Shear failure of anisotropic materials. *Journal of Boston Society of Civil Engineers*, *31*(4), 74-81.

Chattopadhyay, B. C., and Pise, P. J. (1986). Breakout resistance of horizontal anchors in sand. *Soils and Foundations*, 26(4), 16-22.

Cundall, P. A., and Strack, O. D. (1979). A discrete numerical model for granular assemblies. *Géotechnique*, 29(1), 47-65.

Das, B. M., and Seeley, G. R. (1975). Breakout resistance of shallow horizontal anchors. *Journal of the Geotechnical Engineering Division*, 101(9), 999-1003.

Dickin, E.A. (1988). Uplift behavior of horizontal anchor plates in sand. *Journal of Geotechnical Engineering*, 114(11), 1300-1317.

El-Sherbiny, R.M. (2005). *Performance of suction caisson anchors in normally consolidated clay [dissertation]*. Austin, TX: The University of Texas at Austin.

Evans, T.M. and Valdes J.R. (2011). The microstructure of particulate mixtures in one -dimensional compression: numerical studies. *Granular Matter*, 13, 657-669.

Evans, T.M. and Zhang, N. (2015). *Advanced Laboratory and Field Arrays (ALFA) for Marine Energy, Project Checkpoint Report 4.1.1*, December.

Fonseca, J., O'Sullivan, C., Coop, M.R. and Lee, P.D. (2013a). Quantifying the evolution of soil fabric during shearing using directional parameters. *Géotechnique*, 63(6), pp. 487-499.

Fonseca, J., O'Sullivan, C., Coop, M.R. and Lee, P.D. (2013b). Quantifying the evolution of soil fabric during shearing using scalar parameters. *Géotechnique*, 63(10), pp. 818-829.

Frost, J.D., Evans, T.M., Hebeler, G.L., and Giroud, J.P. (2002). Influence of wear mechanisms on geosynthetic interface strengths. In *Geosynthetics: State of the Art-Recent Developments. Proceedings of the Seventh International Conference on Geosynthetics*, 22-27 September, Nice, France. Volume 4.

Frost, J.D., Hebeler, G.L., Evans, T.M., and DeJong, J.T. (2004). "Interface behavior of granular soils." *Engineering Construction and Operations in Challenging Environments Earth and Space 2004: Proceedings of the Ninth Biennial ASCE Aerospace Division International Conference*, League City/Houston, TX, United States, 65.

Gaudin, C., O'Loughlin, S.D., Randolph, M.F. and Lowmass, A.C. (2006). Influence of the installation process on the performance of suction embedded plate anchors. *Géotechnique*, 56(6): 381–391.

Hanna, A., Foriero, A., and Ayadat, T. (2015). Pullout Capacity of Inclined Shallow Single Anchor Plate in Sand. *Indian Geotechnical Journal*, 45(1), 110-120.

Koprivica, S. (2009). Uplift behavior of shallow horizontal plate anchors in sand. *International Journal of Geotechnical Engineering*, 3(4), 485-491.

Kumar, J., and Kouzer, K.M. (2008). Vertical uplift capacity of horizontal anchors using upper bound limit analysis and finite elements. *Canadian Geotechnical Journal*, 45(5), 698-704.

Lambe, T. W., and Whitman, R. V. (2008). *Soil mechanics.* John Wiley and Sons, New York.

Lieng, J.T., Hove, F., and Tjelta, T.I. (1999). Deep Penetrating Anchor: Subseabed deepwater anchor concept for floaters and other installations. In proceedings of the *Ninth International Offshore and Polar Engineering Conference*. International Society of Offshore and Polar Engineers.

Lieng, J. T., Kavli, A., Hove, F., and Tjelta, T. I. (2000). Deep penetrating anchor: further development, optimization and capacity verification. In proceedings of the *Tenth International Offshore and Polar Engineering Conference*. International Society of Offshore and Polar Engineers.

Liu, J., Hu, H., and Yu, L. (2013, June). Experimental Study on the Pull-out Performance of Strip Plate Anchors in Sand. In *The Twenty-third International Offshore and Polar Engineering Conference*. International Society of Offshore and Polar Engineers.

Liu, J., Liu, M., and Zhu, Z. (2011). Sand deformation around an uplift plate anchor. *Journal of Geotechnical and Geoenvironmental Engineering*, 138(6), 728-737.

Medeiros Jr, C. J. (2002). Low cost anchor system for flexible risers in deep waters. In *proceedings of Offshore Technology Conference*, Houston, Paper OTC 14151.

Merifield, R. S., and Sloan, S. W. (2006). The ultimate pullout capacity of anchors in frictional soils. *Canadian Geotechnical Journal*, 43(8), 852-868.

Meyerhof, G. G., and Adams, J. I. (1968). The ultimate uplift capacity of foundations. *Canadian Geotechnical Journal*, 5(4), 225-244.

Mühlhaus, H.B., and Vardoulakis, I. (1987). "Thickness of shear bands in granular materials." *Géotechnique*, 37(3), 271-283.

Murray, E. J., and Geddes, J. D. (1987). Uplift of anchor plates in sand. *Journal of Geotechnical Engineering*, 113(3), 202-215.

Ng, T.T. (2004). Macro-and micro-behaviors of granular materials under different sample preparation methods and stress paths. *International journal of solids and structures*, 41(21), 5871-5884.

O'Loughlin, C. D., Richardson, M. D., and Randolph, M. F. (2009, January). Centrifuge tests on dynamically installed anchors. In *ASME 2009 28th International Conference on Ocean, Offshore and Arctic Engineering* (pp. 391-399). American Society of Mechanical Engineers.

O'Sullivan, C. (2011). *Particulate Discrete Element Modelling: A Geomechanics Perspective*. Applied Geotechnics. Spon Press/Taylor & Francis, New York, NY.

O'Loughlin, C. D., Randolph, M. F., and Richardson, M. (2004). Experimental and theoretical studies of deep penetrating anchors. In proceedings of Offshore Technology Conference, Houston. Paper 16841.

Potyondy, D., and S. Emam. (2014). PFC3D 4.0 Manual Modifications, Itasca Consulting Group, Inc., Technical Memorandum distributed with PFC3D 4.0 executable (February 6, 2014), Minneapolis, Minnesota.

Randolph, M., and Gourvenec, S. (2011). *Offshore geotechnical engineering*. CRC Press, New York, NY.

Rao, K. S. S., and Kumar, J. (1994). Vertical uplift capacity of horizontal anchors. *Journal of Geotechnical Engineering*, 120(7), 1134-1147.

Richardson, M. D., O'Loughlin, C. D., Randolph, M. F., and Gaudin, C. (2009). Setup following installation of dynamic anchors in normally consolidated clay. *Journal of Geotechnical and Geoenvironmental Engineering*, *135*(4), 487-496.

Rothenburg, L. and R. Bathurst (1989). Analytical study of induced anisotropy in idealized granular materials. *Géotechnique.* 39 (4), 601–614.

Rowe and Davis (1982). The behavior of anchor plates in sand. *Géotechnique*. 32(1), 25-41

Salgado, R. (2008). *The engineering of foundations*. New York: McGraw Hill.

Valent, P.J., Taylor, R.J., Atturio, J.M., and Beard, R.M. (1979). Single anchor holding capacities for ocean thermal energy conversion (OTEC) in typical deep sea sediments. *Ocean Engineering*, 6(1), 169-245.

Vesic, A.S. (1969). Breakout resistance of objects embedded in ocean bottom. Duke University, Durham NC.

Wang, J., Dove, J.E., and Gutierrez, M.S. (2007). Discrete-continuum analysis of shear banding in the direct shear test. *Géotechnique*, 57(6), 513–526.

Woodcock, N. (1977). Specification of fabric shapes using an eigenvalue method. *The Geological Society of American Bulletin 88*, 12311236.

Yang, M., Aubeny, C.P., and Murff, J.D. (2011). Behavior of suction embedded plate anchors during keying process. *Journal of Geotechnical and Geoenvironmental Engineering*, 138(2), 174-183.

Yimsiri, S. and K. Soga (2001).Effects of soil fabric on undrained behavior of sands. In S. Prakish (Ed.), *Fourth International Conference on Recent Advances in Geotechnical Earthquake Engineering and Soil Dynamics*, San Diego, California.

Zhang, N and Evans, T. M. (2016). Anchoring of Marine Hydrokinetic Energy Devices: Three Dimensional Simulations of Interface Shear, Geo-Chicago 2016